Article

Gas Sensitive Characteristics of Polyaniline Decorated with Molybdenum Ditelluride Nanosheets

Xinpeng Chen, Xiangdong Chen *, Xing Ding * and Xiang Yu

School of Information Science and Technology, Southwest Jiaotong University, Chengdu 610097, China; cxp@my.swjtu.edu.cn (X.C.); yuxiang@my.swjtu.edu.cn (X.Y.)
* Correspondence: xdchen@swjtu.edu.cn (X.C.); xding@swjtu.edu.cn (X.D.); Tel.: +86-138-8181-6882 (X.C.)

Abstract: In this work, hydrochloric acid (HCl)-doped molybdenum ditelluride ($MoTe_2$) nanosheets/polyaniline (PANI) nanofiber composites are prepared by in situ chemical oxidation polymerization, and then the composites are deposited on interdigital electrodes (IDEs) to fabricate a NH_3 gas sensor. Morphological analysis of the composites reveals that the PANI fibers are deposited on 2D $MoTe_2$ sheets, showing a porous mesh microstructure structure with a more continuous distribution of PANI layer. FTIR spectrum analysis indicates the interaction between the $MoTe_2$ nanosheets and the PANI in the $MoTe_2$/PANI composites. The results demonstrate that the as-prepared $MoTe_2$/PANI composites exhibit higher response than the pure PANI, in particular, the 8 wt.% $MoTe_2$/PANI composites display about 4.23 times enhancement in response value toward 1000 ppm NH_3 gas compared with the pure PANI. The enhanced NH_3 gas-sensitive properties may be due to the increasing surface area of $MoTe_2$/PANI composite films and the possible interaction of the P-N heterojunctions formed between PANI and the 2H-$MoTe_2$ nanosheets.

Keywords: $MoTe_2$ nanosheets; polyaniline; NH_3 gas sensor; P-N heterojunctions; ammonia

1. Introduction

Ammonia (NH_3) gas is widely used in the chemical industry, light industry, chemical fertilizer and pharmaceutical industries [1]. No matter the field, be it air quality monitoring or health care, it is imperative to the real-time detection of NH_3 gas.

Among the large number of NH_3 gas-sensitive materials, polyaniline (PANI), as a member of conducting polymer family, has been widely studied due to its operation at room temperature; ease of processing; and unique, simple and reversible acid/base doping/dedoping chemistry [2,3]. However, as a gas sensitive material, PANI has some drawbacks, such as relatively low sensitivity and long response/recovery time, which seriously affect its practical application in NH_3 gas sensors [4–6]. In order to further improve the performance of PANI-based NH_3 gas sensors, a number of works on PANI incorporated with various materials (e.g., metal oxide [7], metallic nanoparticles [8], carbon nanotubes [9], graphene [4,10], MXene [11] and TMDs [12], etc.) have been reported.

Among the above materials, transition metal dichalcogenides (TMDs), such as MoS_2, WS_2, $MoSe_2$ and $MoTe_2$, have received considerable attention in the field of chemical sensors owing to their unique structural and electrical properties, such as high specific surface area and surface energy level [13–16]. Jha et al. [12] reported WS_2/PANI composite-based sensors with enhanced sensitivity and selectivity toward NH_3 gas at room temperature. Liu et al. [17] presented a porous polyaniline/tungsten disulfide (PANI/WS_2) nanocomposite film for the detection of NH_3 gas at ppm level. Zhang et al. [18] synthesized polyaniline/multiwall carbon nanotubes/molybdenum disulfide ternary nanocomposites (PANI/MWCNTs/MoS_2) and PANI/MoS_2 binary nanocomposites for NH_3 gas sensing under room temperature, respectively.

As one of the promising TMDs materials, the $MoTe_2$ lattice has a three-layer structure, in which a hexagonal plane of Mo atoms is sandwiched between two separate hexagonal

planes composed of Te atoms, and each layer is bonded together by weak Van der Waals force [19,20]. Iman Shackery et al. [21] reported a gas sensor based on α-MoTe$_2$ with a back-to-back diode structure, and response tests to NH$_3$ gas and NO$_2$ gas showed that this type of sensor has a better response performance for NH$_3$ gas than it does for NO$_2$ gas, which suggested that MoTe$_2$ could be a candidate for NH$_3$ gas sensing applications. Feng et al. [16] developed a field-effect tube (FET) gas sensor based on MoTe$_2$ flakes (thickness about 6.5 nm) and tested its sensitive properties to NH$_3$ gas and NO$_2$ gas; the results show that the detection sensitivity of MoTe$_2$ for NH$_3$ is higher than that of NO$_2$ and the recovery time in NH$_3$ gas is shorter than that in NO$_2$ gas. However, the more complicated preparation process and the weaker output signal limit the further application of these devices.

Compared to other TMDs, MoTe$_2$ has a larger bond length, lower binding energy and a narrower band gap (about 1.0 eV), which is more favorable for the adsorption of gas molecules [17,22]. Meanwhile, the two crystal structures of MoTe$_2$, 2H (hexagonal) as a semiconductor and 1T' (distorted octahedral) as a metal type [22], make it beneficial to employ the synergistic effect between multiple materials to facilitate enhanced gas-sensitive properties when incorporated with other materials [15,22]. Moreover, the MoTe$_2$ nanosheet is a 2D material and the flexible PANI is incorporated with the 2D material, so that the 2D material can act as a structural support, thus avoiding the excessive stacking of the PANI matrix and facilitating the formation of a larger contact area with analyte molecules [10]. However, there are few reports of PANI incorporated with MoTe$_2$ for NH$_3$ gas sensor.

In the present work, MoTe$_2$/PANI composites are prepared by a simple in situ chemical oxidative polymerization of aniline on N type 2H-MoTe$_2$ nanosheets. Then, NH$_3$ gas sensors are formed by coating the MoTe$_2$/PANI composites films onto the gold interdigital electrodes (IDE). The experimental results show that the NH$_3$ gas-sensitive properties of the PANI based composites are further enhanced after being hybridized with MoTe$_2$. Finally, the possible sensitive mechanism of the prepared sensor toward NH$_3$ gas is proposed in detail.

2. Experimental

2.1. Materials and Reagents

An N type 2H-MoTe$_2$ nanosheets dispersion (0.5 mg/mL) was purchased from Nanjing MKNANO Tech. Co., Ltd (Nanjing, China). Aniline monomers, ammonium persulfate (APS), hydrochloride (HCl) and ethanol were purchased from Chengdu Kelong Chemical Reagents Co., Ltd. (Chengdu, China). All materials and reagents used in the experiment were analytical grade without further treatment, except for aniline monomers, which were purified by reduced pressure distillation before use. Deionized (DI) water (18.2 MΩ cm resistivity, Milli-Q) was used in the experiments.

2.2. Synthesis of MoTe$_2$/PANI Composites

MoTe$_2$/PANI composites were synthesized by an in situ oxidative polymerization method, which was reported in our previous work [23]. In this typical process, a 30 mL MoTe2 nanosheet dispersion, 0.2 mL (0.002 mol) aniline monomer and 8.3 mL (1 M) HCl solution were mixed with 50 mL DI water and sonicated for 0.5 h. Then the mixture was transferred to an ice bath (0–5 °C) with continuous magnetic stirring. After that, 0.465 g APS (0.002 mol) was dissolved in 20 mL DI water and gradually dropped into the above mixture. Subsequently, the polymerization reaction occurred. The mixture was kept for 15 h at 0–5 °C and the MoTe$_2$/PANI composites was obtained, showing a dark green color. Next, the obtained precipitate was filtered and rinsed with DI water and ethanol for several times, then dried in a vacuum oven at 25 °C for 24 h. A part of the precipitate was collected for characterization.

For comparison, the pure PANI and MoTe$_2$/PANI composites with the various volumes of nanosheet dispersion (5 mg and 60 mg) were synthesized utilizing the same process.

For the prepared $MoTe_2$/PANI composites, the mass ratios of $MoTe_2$ nanosheets (5 mg, 15 mg and 30 mg) to PANI were calculated to be 2.7 wt.%, 8 wt.% and 16 wt.%, respectively.

2.3. Characterization

The surface microstructure and morphology of the as-synthesized materials was elucidated via scanning electron microscopy (FE-SEM, GeminiSEM 300, ZEISS company, Oberkochen, Baden-Württemberg, Germany) and high-resolution transmission electron microscopy (HRTEM, JEM1200EX, JEOL company, Tokyo, Japan). Fourier transform infrared spectra (FTIR) of the as-synthesized materials were recorded on a PerkinElmer Frontier spectrometer with the samples were dispersed and pressed with KBr pellets over the wavenumber range of 400–4000 cm^{-1} at room temperature.

2.4. Fabrication of NH_3 Gas Sensor

The NH_3 gas sensor was fabricated by coating the as-synthesized sensitive materials on gold interdigital electrodes. The specific fabrication process is a two-step process as follows:

The first step was to fabricate the gold interdigital electrodes. First, a layer (300 nm) of SiO_2 film was thermally grown on the silicon wafer as a passivation layer. A layer (100 nm) of titanium (Ti) layer and a layer (100 nm) of gold (Au) were successively deposited on the SiO_2 passivation layer by magnetron sputtering, in which the Ti layer played a role in enhancing the adhesion between the SiO_2 passivation layer and the Au electrode. Subsequently, a layer of photoresistance is applied to the silicon wafer and the interdigitated electrode pattern was photo-lithographically defined by using the mask. Each interdigital electrode was composed of 10 pairs of fingers with 25 μm width and 25 μm gaps, and the size of electrodes area was 4 mm × 6 mm. After the developing and wet etching processes, the silicon wafers containing gold interdigitated electrodes were obtained. Finally, the silicon wafer was then diced into individual chips. Before the deposition of sensitive materials, gold interdigitated electrodes were successively rinsed with DI water and ethanol and dried in a vacuum desiccator at room temperature for 24 h.

The second step was to apply the sensitive materials to the gold interdigitated electrodes. First, the as-synthesized $MoTe_2$/PANI composites and pure PANI were, respectively, dispersed ultrasonically into a mixture of DI water and ethanol (1 mg/mL) for 15 min to obtain stable suspension. Then, 4 microliters (μL) of the $MoTe_2$/PANI composites, PANI suspension and $MoTe_2$ Nanosheets dispersion were, respectively, applied onto the interdigitated electrodes by the drop-coating method using a micropipette. Finally, the well-coated interdigitated electrodes were dried in a vacuum desiccator at room temperature for 3 h to obtain the gas sensors.

In order to investigate a possible synergies interaction between the P type PANI and N type $MoTe_2$ nanosheets in the $MoTe_2$/PANI composites, a layered heterostructured sensor composed of 2H-$MoTe_2$ nanosheet films and PANI films was fabricated by sequentially apply the N type 2H-$MoTe_2$ nanosheets dispersion and PANI dispersion onto the channel and electrode of the planar electrode, as shown schematically in Figure 1.

Figure 1. Schematic diagram of the layered heterostructured sensor device composed of 2H-$MoTe_2$ film and PANI film.

2.5. Gas-Sensing Test

A gas-sensing test was carried out by exposing the sensors to various concentrations of NH_3 gas under laboratory conditions (62.7 ± 3% RH, 22 ± 2 °C). The NH_3 gas sensing measurement systems used in this work was described in our previous study [23]. The

sensor was placed in a test chamber (1 L in volume) with an inlet and an outlet. Standard NH_3 gas (10,000 ppm, N_2 was used as the balance gas) was purchased from NIMTT (Chengdu, China). Various NH_3 gas concentration (ranging from 10 ppm to 1000 ppm) environments were achieved by regulating a mass flow system consisting of a 5 SCCM and a 500 SCCM mass flowmeters. Clean air was used to clear the residual NH_3 gas in the test chamber before and after the gas-sensing test. The resistance of the sensor was monitored and measured in real time by a digital multimeter (34461A, Keysight company, Cleveland, OH, USA), which was connected to a computer via the USB interface for data acquisition, and the resistance was recorded at a rate of once every 500 milliseconds. The current–voltage (I-V) characteristics of sensor are measured with a computerized source meter (Keithley 2400, Tektronix, Beaverton, OR, USA).

The response value (S) of the sensor is defined as:

$$S = \frac{R}{R_0} = \frac{R_1 - R_0}{R_0} \tag{1}$$

where R_1 and R_0 are the resistance of the sensor when exposed to the given concentration of NH_3 gas and the clean air, respectively. The response times and recovery times of the sensor are calculated as the times to attain 90% of total resistance change.

3. Results and Discussion

3.1. The Characterization of Morphology and Microstructure

SEM images of pure PANI, $MoTe_2$ nanosheets and $MoTe_2$/PANI composites are shown in Figure 2a–c, respectively. High-resolution SEM image of $MoTe_2$/PANI composites (100 nm scale) is shown in Figure 2d. As can be seen in Figure 2b, it is clear that a large number of 2D layered sheets with sizes of tens to hundreds of nanometers stack together. In Figure 2a,c, it can be found that both of pure PANI and $MoTe_2$/PANI composites exhibit an interconnected mesh nanofiber morphology. However, it can also be clearly seen in the SEM images of $MoTe_2$/PANI composites in Figure 2c,d that the PANI fibers are covered and deposited on the lamellar $MoTe_2$ nanosheets, which indicates that there is good contact between PANI nanofibers and $MoTe_2$ nanosheets, facilitating the formation of interactions between different components at interface. On the other hand, compared to the microstructure of pure PANI in Figure 2a, the deposition of PANI fibers on 2D nanosheets in the $MoTe_2$/PANI composites reduces the stacking in the vertical direction and expands the distribution area in the planar direction, resulting in a relatively more uniform distribution of PANI layers. For the application of gas-sensitive materials, this microstructure facilitates a further increase in the contact area with the gas molecules, thus achieving a further improvement in gas-sensitive properties [10].

HRTEM images of pure PANI, $MoTe_2$ nanosheets and $MoTe_2$/PANI composites are shown in Figure 3a–c, respectively. The lamellar structure of $MoTe_2$ nanosheets with a size of about several hundred nanometers can be clearly observed in Figure 3b; the reticulated structural morphology of PANI nanofibers with the diameter of about several tens of nanometers can be observed in Figure 3a; the PANI nanofibers with the reticulated structural morphology can also be clearly observed in Figure 3c; however, compared with Figure 3a, the PANI nanofibers in Figure 3c are deposited on the lamellar $MoTe_2$ nanosheets, and the $MoTe_2$ nanosheets are well distributed without obvious agglomeration. This difference in microstructure morphology is also consistent with SEM characterization in Figure 2a–c above, which suggests a better spatial distribution uniformity of PANI layers in the $MoTe_2$/PANI composites.
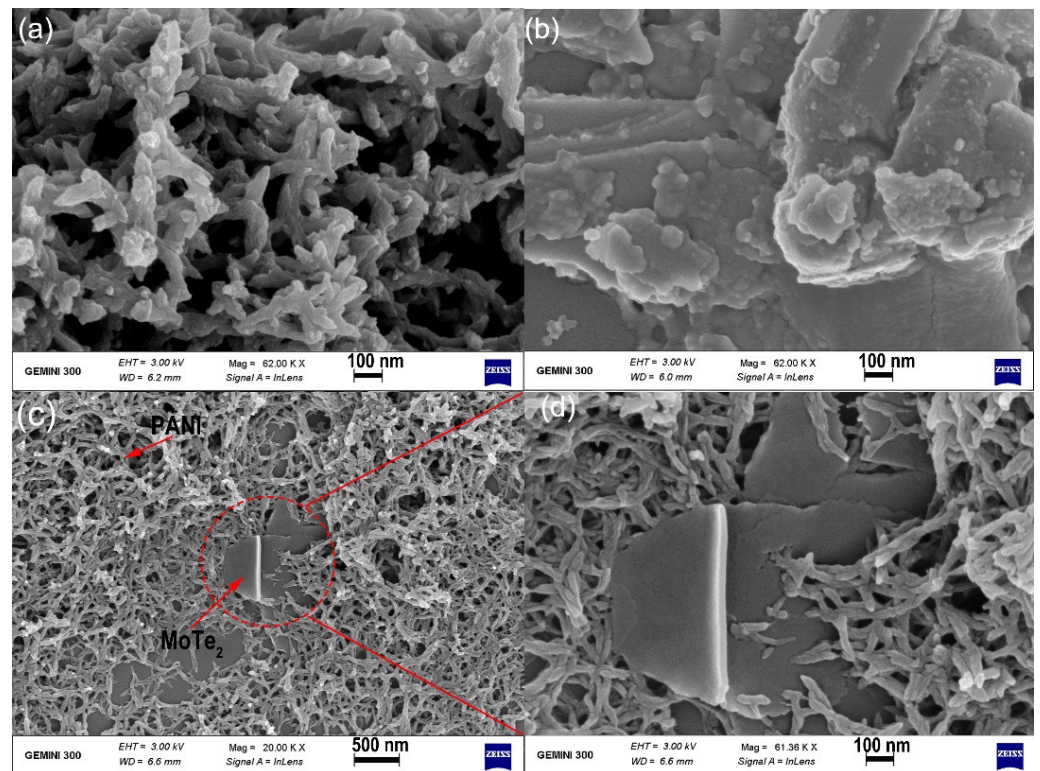
Figure 2. SEM images of (**a**) pure PANI, (**b**) $MoTe_2$ nanosheets, (**c**) $MoTe_2$/PANI nanocomposites; (**d**) high-resolution SEM image of $MoTe_2$/PANI nanocomposites (100 nm scale).
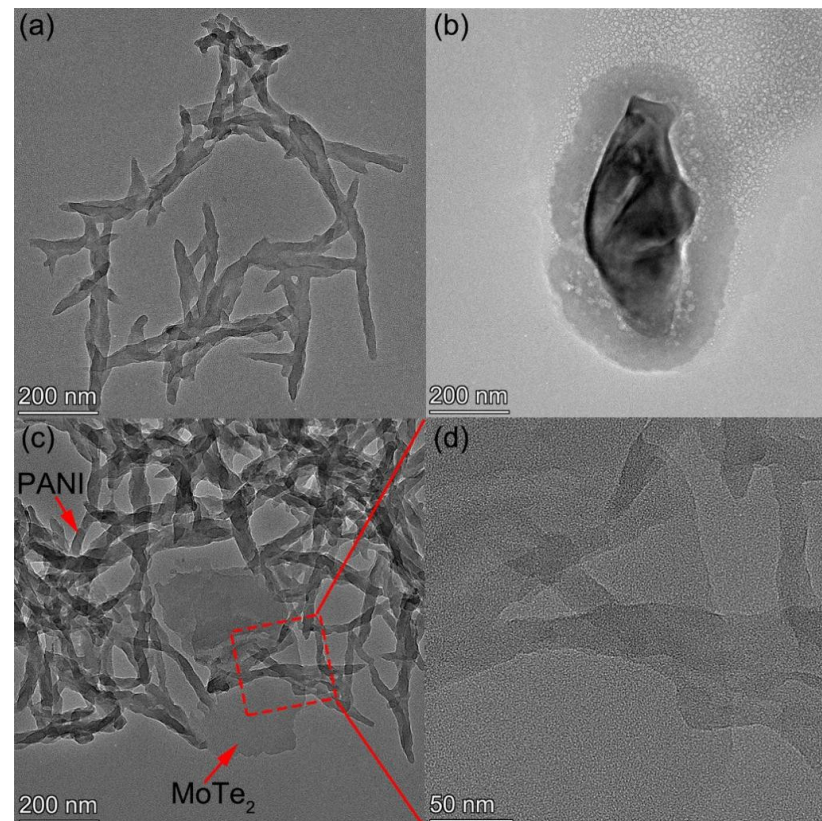
Figure 3. High-resolution TEM (HRTEM) images of (**a**) pure PANI, (**b**) $MoTe_2$ nanosheets, (**c**) $MoTe_2$/PANI nanocomposites (200 nm scale); (**d**) HRTEM image of $MoTe_2$/PANI nanocomposites (50 nm scale).

3.2. FTIR Analysis

　　The FTIR spectrum of $MoTe_2$ nanosheets, pure PANI and 8 wt.% $MoTe_2$/PANI composites are shown in Figure 4. The FTIR spectra of 8 wt.% $MoTe_2$/PANI composites, as well as $MoTe_2$ nanosheets, show a similar characteristic peak, both around 669.5 cm^{-1}, which is attributed to the vibration of the Mo–Te bond [22]. For pure PANI, the characteristic peak at 795.9 cm^{-1} corresponds to the out-of-plane bending vibration of C-H bond of the para-aromatic ring, the characteristic peak at 1113.2 cm^{-1} is attributed to the in-plane bending vibration of C-H bond, the characteristic peak at 1241.4 cm^{-1} corresponds to stretching vibration of C≡N bond of aromatic secondary amine and the characteristic peak at 1296.8 cm^{-1} is ascribed to the stretching vibration of the C-N bond, the characteristic peaks at 1484.4 cm^{-1} and 1567.8 cm^{-1} are assigned to stretching vibration of C=C bond and stretching vibration of C=N of quinoid ring, respectively [10,24–27]. All these main characteristic peaks above can be observed in the FTIR spectrum of 8 wt.% $MoTe_2$/PANI composites with similar peaks, which further confirms that the PANI component in both pure PANI and $MoTe_2$/PANI composites prepared in this work exist in the form of the highly conductive emeraldaniline salt [26,28]. Moreover, the main characteristic peaks of doped PANI observed in the FTIR spectrum of 8 wt.% $MoTe_2$/PANI composites have slight shifts compared to the position of pure PANI, which indicates the interaction between the $MoTe_2$ nanosheets and the PANI matrix in the $MoTe_2$/PANI composites [28,29].
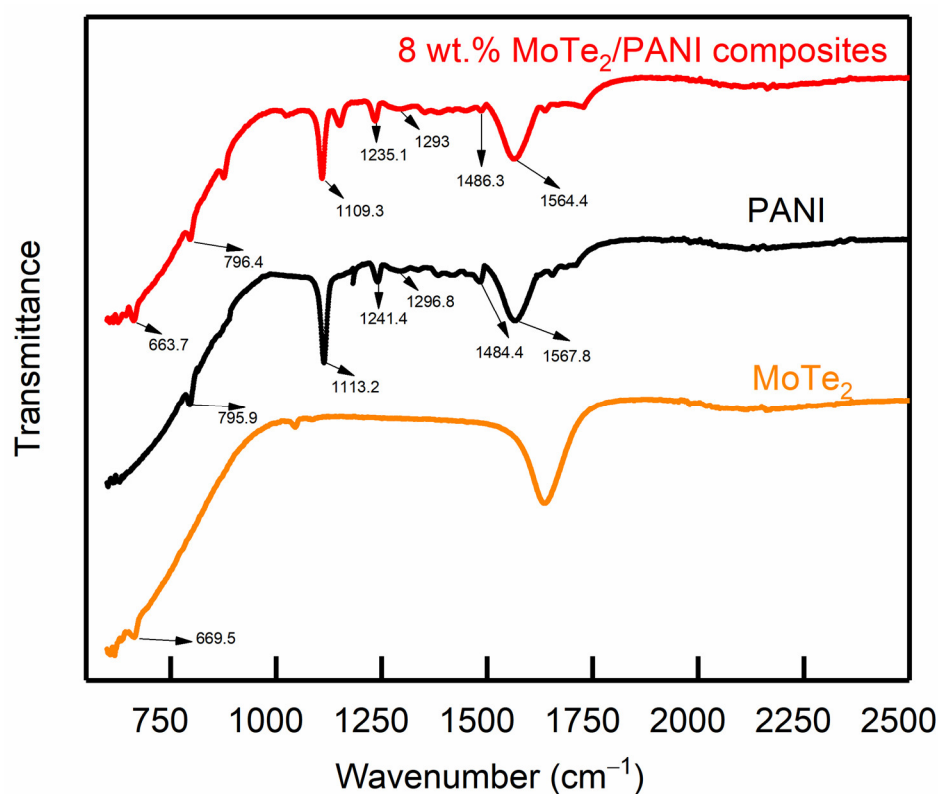
Figure 4. FTIR spectrum of $MoTe_2$ nanosheets, pure PANI and $MoTe_2$/PANI nanocomposites.

3.3. NH3 Gas Sensing Properties

3.3.1. Gas Response

　　The sensor response to NH_3 gas is achieved by switching the response/recovery cycle between different concentrations of NH_3 gas and air. The transient resistance variation of the sensors toward NH_3 gas varied from 10 to 1000 ppm are shown in Figure 5. It can be observed that the resistance value of the sensor based on pure $MoTe_2$ nanosheets shows hardly any significant changes when exposed to various concentrations of NH_3 gas. However, the resistance values of sensors based on pure PANI and $MoTe_2$/PANI

composites increase rapidly with increasing NH_3 gas concentrations and gradually reach to saturation, and then return to the approximate baseline state after the test chamber is refilled with air in each response/recovery cycle. Specifically, when the concentration of NH_3 gas is varied from 0 to 1000 ppm, the resistance of the $MoTe_2$/PANI composites sensors changes from 1.19 Kohm to 66.8 Kohm (2.7 wt.% $MoTe_2$/PANI composites composites), 27.7 Kohm to 2961.1 Kohm (8 wt % $MoTe_2$/PANI composites), 1.87 Kohm to 148.1 Kohm (16 wt.% $MoTe_2$/PANI composites) and the resistance of the pure PANI sensor changes from 5.34 Kohm to 141.1 Kohm.
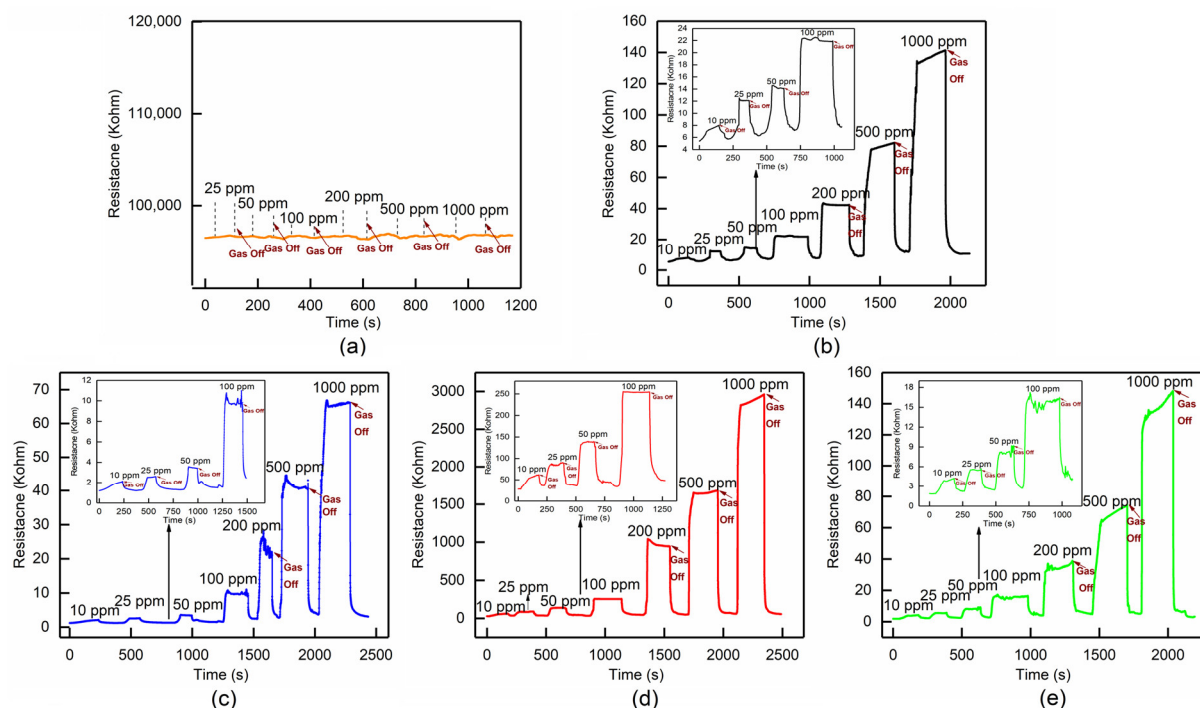
Figure 5. Transient resistance of gas sensors based on (**a**) pure $MoTe_2$ nanosheets, (**b**) pure PANI, (**c**) 2.7 wt.% $MoTe_2$/PANI composites, (**d**) 8 wt.% $MoTe_2$/PANI composites and (**e**) 16 wt.% $MoTe_2$/PANI composites when exposed to various concentrations of NH_3 gas in a laboratory environment.

Regarding the data in Figure 5, the response values of sensors prepared in this work toward different concentrations of NH_3 gas are obtained and collected in Table 1, of which these response values are also demonstrated in Figure 6. Taking the response at a 1000 ppm concentration of NH_3 gas as an example, the responses of 2.7 wt.% $MoTe_2$/PANI composites, 8 wt.% $MoTe_2$/PANI composites and 16 wt.% $MoTe_2$/PANI composites sensors are 2.18, 4.23 and 3.11 times as much as those of pure PANI-based sensor, respectively. This result indicates that the response of $MoTe_2$/PANI composites sensors toward NH_3 gas have been significantly improved compared to that of a pure PANI sensor. This implies that enhanced response of the $MoTe_2$/PANI composites toward NH_3 gas has been achieved by the introduction of $MoTe_2$ nanosheets.

Table 1. The response values of sensors prepared in this work regarding NH_3 gas.

NH_3 Gas Concentration Response	10 ppm	25 ppm	50 ppm	100 ppm	200 ppm	500 ppm	1000 ppm
pure PANI	0.48	1.24	1.69	3.15	6.91	14.12	25.01
2.7 wt.% $MoTe_2$/PANI composites	0.76	1.19	1.99	7.16	17.12	33.9	54.44
8 wt.% $MoTe_2$/PANI composites	1.23	2.24	4.12	8.16	35	59.62	105.9
16 wt.%$MoTe_2$/PANI composites	1.14	1.97	3.37	7.5	19.1	38.48	77.99
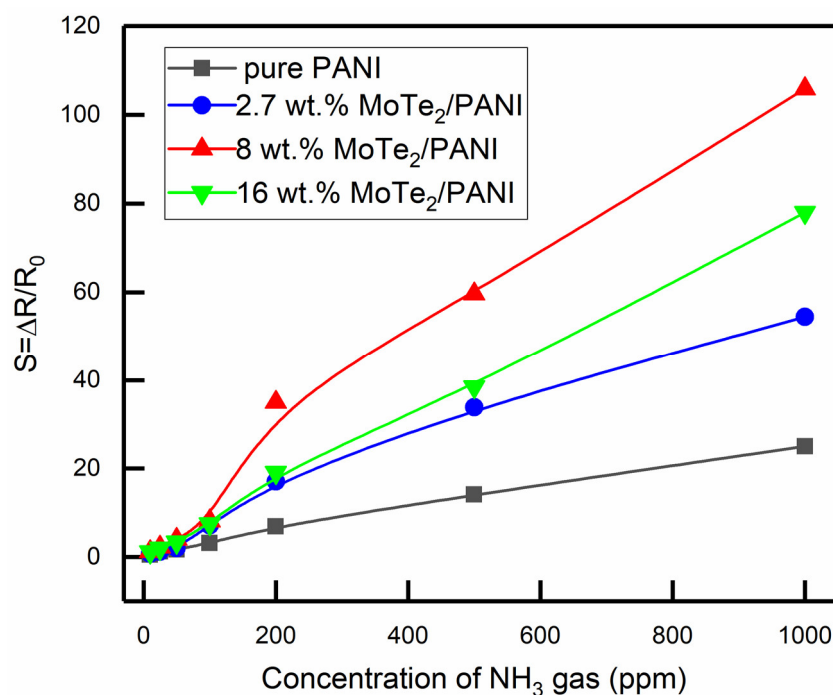
Figure 6. Response of pure PANI sensor and $MoTe_2$/PANI composites sensors as a function of NH_3 gas concentration at laboratory environment.

The response data in Figure 6 also reveals the relationship between the number of $MoTe_2$ nanosheets and the response of $MoTe_2$/PANI composites sensors to NH_3 gas to some extent. The response of $MoTe_2$/PANI composites sensors to NH_3 gas does not always increase with the increase of $MoTe_2$ nanosheet amounts. When the mass ratio of $MoTe_2$ nanosheets to PANI is about 8 wt.%, the $MoTe_2$/PANI composites sensor has the maximum response to NH_3 gas.

3.3.2. Response and Recovery Times

The dynamic response and recovery of the gas sensors based on pure PANI and $MoTe_2$/PANI composites to 100 ppm concentration of NH_3 gas are shown in Figure 7, respectively. It is estimated that the response times (T_1) of the sensors based on pure PANI and $MoTe_2$/PANI composites with various $MoTe_2$ nanosheets amounts are about 36 s, 25 s, 26 s and 25 s, and the corresponding recovery times (T_2) are about 27 s, 12 s, 24 s and 24 s, respectively (as shown in Table 2). It can be seen that the response times of $MoTe_2$/PANI composites sensors are usually shorter than those of pure PANI sensors. Therefore, the addition of $MoTe_2$ nanosheets into the PANI matrix can allow the composites sensitive film to exhibit a faster response/recovery speed. When combining the analysis of the morphology with the microstructure of $MoTe_2$/PANI composites described in Section 3.1, the improvement in response/recovery times may be ascribed to the fact that the PANI nanofibers are covered and deposited on the lamellar $MoTe_2$ nanosheets during the in situ polymerization process, resulting in a more continuous distribution and increased surface area. It provides more active sites for the adsorption of the NH_3 gas molecules, thus accelerating the response/recovery rate and reducing the response/recovery times.

The NH_3 gas-sensitive properties of the $MoTe_2$/PANI composites sensor in this work in comparison with some NH_3 gas sensors reported recently are summarized in Table 3.
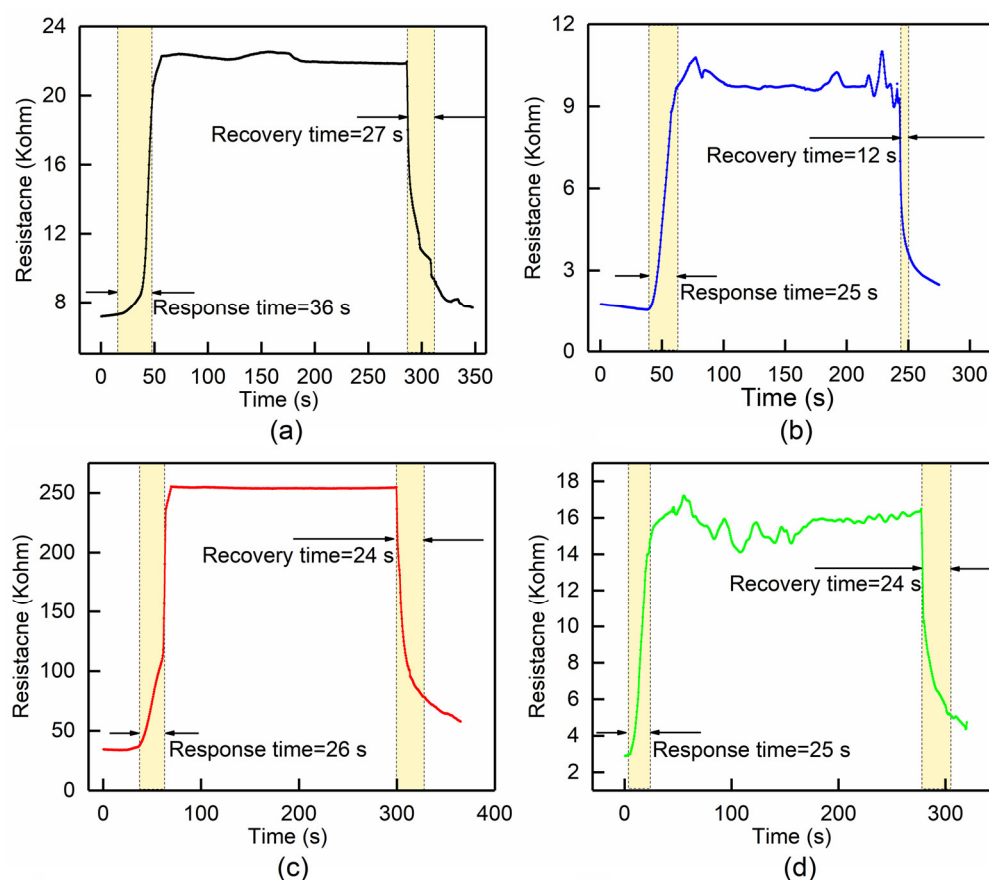
Figure 7. Dynamic response–recovery curves of gas sensors based on (**a**) the pure PANI, (**b**) 2.7 wt.% MoTe$_2$/PANI composites, (**c**) 8 wt.% MoTe$_2$/PANI composites and (**d**) 16 wt.% MoTe$_2$/PANI composites when exposed to a 100 ppm concentration of NH$_3$ gas in a laboratory environment.

Table 2. Response times (T1) and recovery times (T2) of sensors under 100 ppm NH$_3$ gas.

Sensitive Film	Pure PANI	2.7 wt.% MoTe$_2$/PANI	8 wt.% MoTe$_2$/PANI	16 wt.% MoTe$_2$/PANI
Response times (T$_1$)	36 s	25 s	26 s	25 s
Recovery times (T$_2$)	27 s	12 s	24 s	24 s

Table 3. Comparison of MoTe$_2$/PANI composites based NH3 gas sensor and those reported in the literature.

Material	Response (×100%)	T$_1$ (s)	T$_2$ (s)	Type of Transducer	Reference
PANI/GO/PANI/ZnO	38.31%@100 ppm	30	—	Impedance	[30]
PANI-α-Fe$_2$O$_3$	72%@100 ppm	50	1575	Resistive	[31]
PANI/WS$_2$	81%@200 ppm	260	790	Resistive	[12]
PAni-WO$_3$	158%@100 ppm	39	377	Resistive	[32]
3D RGO/PANI hybrid	10.8%@100 ppm	370	675	Resistive	[33]
PANI/Nb$_2$CTx nanosheets	301%@100 ppm	105	143	Voltage	[34]
MoTe$_2$/PANI	816%@100 ppm	25	24	Resistive	This work

3.3.3. Repeatability and Selectivity

In this work, repeatability and selectivity tests were carried out for the 8 wt.% MoTe$_2$/PANI composites sensor. Figure 8a shows the response of the 8 wt.% MoTe$_2$/PANI composites sensor when exposed to a 100 ppm concentration of NH$_3$ gas for three repeated cycles; it can be found that there is no significant deviation during the cycle testing of the

sensor, which indicates a good reproducibility of the sensor. Figure 8b shows the response of the 8 wt.% $MoTe_2$/PANI composites sensor to 100 ppm concentrations of NH_3 gas, methane (CH_4), ethanol (C_2H_5OH), acetone (CH_3COCH_3), formaldehyde (CH_2O), benzene (C_6H_6) and nitrogen dioxide (NO_2), respectively. It is clear that the response of the 8 wt.% $MoTe_2$/PANI composites sensor toward NH_3 gas is significantly higher than that of the other gases measured.
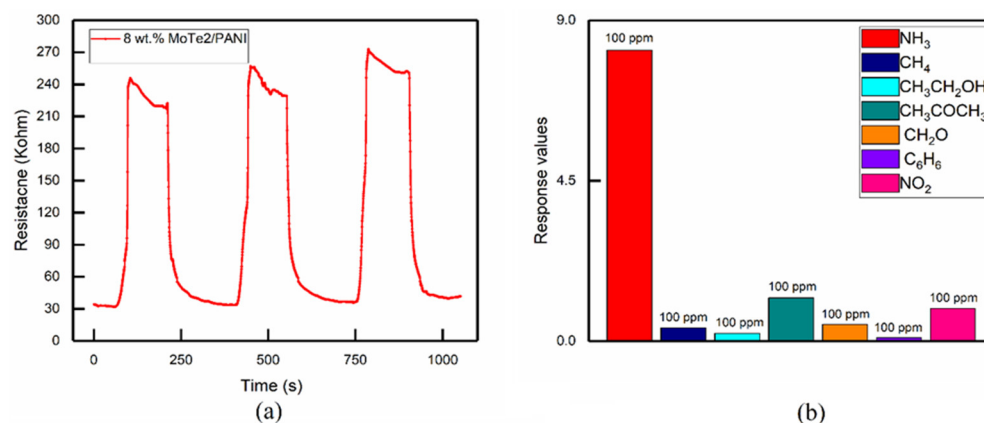
Figure 8. (**a**) Repeatability and (**b**) selectivity of 8 wt.% $MoTe_2$/PANI composites gas sensor.

3.3.4. Enhanced Mechanism for the Gas-Sensitive Response of $MoTe_2$/PANI Composites

From the results obtained in Section 3.3.1, $MoTe_2$ nanosheets do not show a significant response behavior to NH_3 gas, but after compounding with PANI significantly enhance the NH_3 gas-sensitive response of the $MoTe_2$/PANI composites. This potential NH_3 gas-sensitive mechanism is not fully understood, but these enhanced gas-sensitive properties may be due to the morphology of the composites and the synergistic interaction between the components of the composites.

According to the morphology and microstructure analysis of $MoTe_2$/PANI composites, as discussed in Section 3.1, it is evident that the PANI nanofibers are polymerized on 2D $MoTe_2$ nanosheets in the composites with the introduction of $MoTe_2$ nanosheets. Moreover, due to the deposition of PANI nanofibers on 2D nanosheets in the composites, the stacking in the vertical direction is reduced and the distribution area in the planar direction is expanded, which provides a large number of active sites for the adsorption of NH_3 gas molecules onto the composites films.

In order to further investigate the enhanced gas-sensitive mechanism of $MoTe_2$/PANI composites, the characteristics of the layered heterostructured sensor is tested. The I-V characteristic curves of the layered heterostructured sensor when exposed to a 500 ppm concentration of NH_3 gas are shown in Figure 9. It can be observed that the I-V characteristic curves of the layered heterostructured sensor exhibit non-ohmic characteristics and show a certain rectification behavior of a P-N heterojunction within the voltage range of −1~+1 V, which indicates a certain degree of heterojunction interaction between N-type 2H-$MoTe_2$ nanosheets and P-type PANI [35,36]. This result is consistent with the observation of a certain degree of interaction between the $MoTe_2$ nanosheets and the PANI in the FTIR spectrum in Section 3.2.

The formation of the heterojunction may be related to the energy level structure of the two materials (as shown in Figure 10). The positions of the lowest unoccupied molecular orbital (LUMO) and the highest occupied molecular orbital (HOMO) in PANI, as well as the positions of the conduction bands (Ec) and valence band (Ev) in the 2H-$MoTe_2$ nanosheets and the positions of their Fermi energy levels relative to the vacuum energy levels, are shown in Figure 10. According to previous reports, the band gaps of PANI and 2H-$MoTe_2$ are 2.8 Ev and 1.0 Ev, respectively [16,37]. When PANI nanofibers are polymerized and deposited on 2H-$MoTe_2$ nanosheets, due to gradient difference in carrier concentrations at the interface between PANI and $MoTe_2$ nanosheets, the majority carriers (holes) in PANI

and the majority carriers (electrons) in 2H-MoTe$_2$ nanosheets diffuse along their opposite directions until reaching an equilibrium at the Fermi energy level and P-N heterojunctions are subsequently formed at the interface between PANI and MoTe$_2$ nanosheets [18,38]. When the MoTe$_2$/PANI composites are exposed to NH$_3$ gas, NH$_3$ molecules capture protons from the composites, leading to a decrease in the doping concentrations of the PANI component in the composites, which not only results in an increase for the intrinsic resistance of PANI but also in a broadening of depletion layer of the P-N heterojunction. It may result in a further increase in the resistance of the composites, which enhances the NH$_3$ gas-sensitive response of the MoTe$_2$/PANI composites sensor [39].
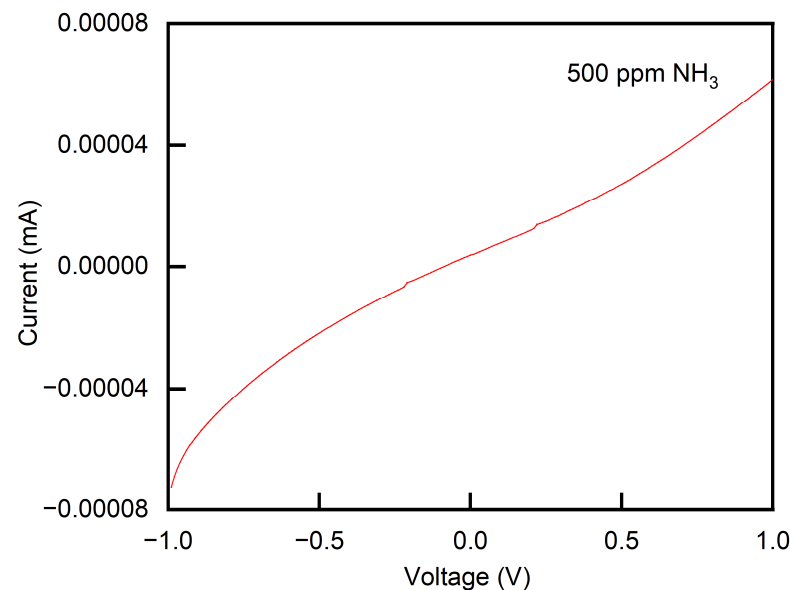
Figure 9. I-V characteristic curve of the layered heterostructured sensor composed of 2H-MoTe$_2$ film and PANI film when exposed to exposed to a 500 ppm concentration of NH$_3$ gas.
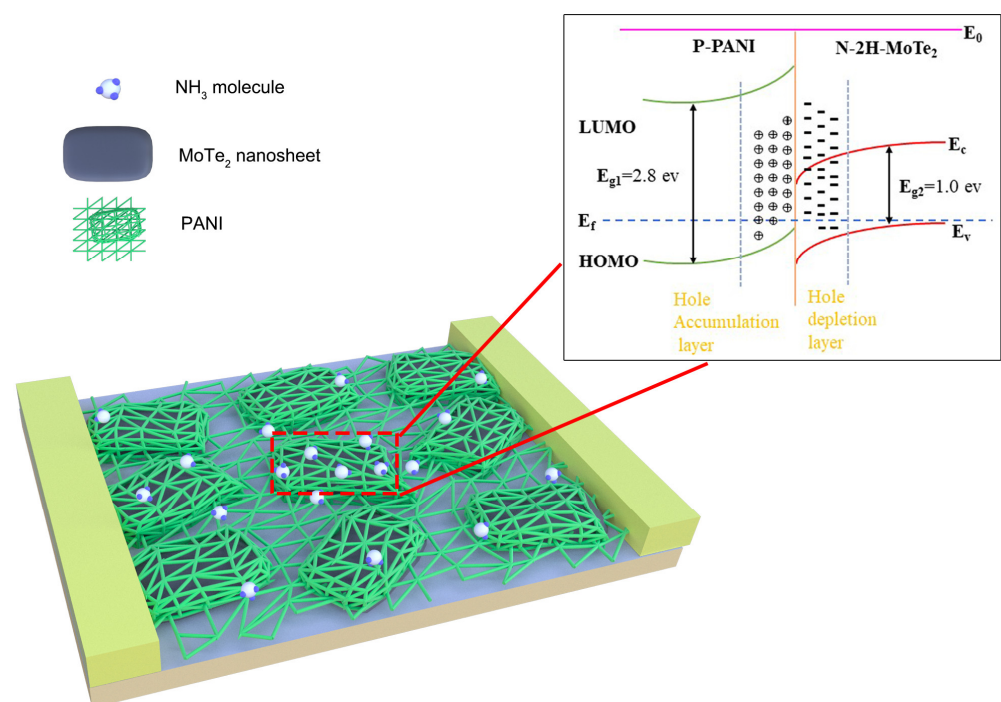
Figure 10. Schematic diagram of band structure at the interface between MoTe$_2$ nanosheets and PANI nanofibers of MoTe$_2$/PANI composites.

4. Conclusions

MoTe$_2$/PANI nanocomposites were prepared by in situ chemical oxidation polymerization and the NH$_3$ gas sensor was assembled by using MoTe$_2$/PANI nanocomposites combined with an IDE transducer. It was found that PANI nanofibers cover the lamellar MoTe$_2$ nanosheets and form a porous mesh microstructure, which increases the surface area of PANI layer and provides more active sites for the adsorption of gas molecules. The sensitive characteristics of NH$_3$ gas show that the MoTe$_2$/PANI composites sensors have better response to NH$_3$ gas over the concentration range of 10–1000 ppm than the pure PANI sensors. In particular, the 8 wt.% MoTe$_2$/PANI composite sensor shows the highest response (4.23 times as much as the pure PANI sensor at 1000 ppm NH$_3$ gas). The response of MoTe$_2$/PANI nanocomposites is also faster than that of pure PANI sensors. Beyond the morphological and microstructure analysis of the MoTe$_2$/PANI composites, the effect of introducing 2D MoTe$_2$ nanosheets to the enhanced NH$_3$ gas-sensitive properties of PANI is also discussed in this work in terms of the possible formation of P-N heterojunctions at the interface between MoTe$_2$ nanosheets and PANI.

Author Contributions: X.C. (Xinpeng Chen): Conceptualization, methodology, investigation and writing—original draft and revising; X.C. (Xiangdong Chen): Conceptualization, funding acquisition, resources, supervision and writing—review and editing. X.D.: Provide help in improving the manuscript regarding format, language and figures; X.Y.: Provided help in improving the manuscript regarding format, language and figures. All authors have read and agreed to the published version of the manuscript.

Institutional Review Board Statement: Not applicable.

Informed Consent Statement: Not applicable.

Data Availability Statement: The data presented in this study are available on request from the corresponding author. The data are not publicly available due to the laboratory confidentiality requirements.

Conflicts of Interest: The authors declare no conflict of interest.

References

1. Li, X.; Li, T.; Ma, Y.; Wei, Q.; Qiu, W.; Guo, H.; Shi, X.; Zhang, P.; Asiri, A.M.; Chen, L.; et al. Boosted electrocatalytic N$_2$ reduction to NH$_3$ by defect-rich MoS$_2$ nanoflower. *Adv. Energy Mater.* **2018**, *8*, 1801357. [CrossRef]
2. Virji, S.; Huang, J.; Kaner, R.B.; Weiller, B.H. Polyaniline nanofiber gas sensors: Examination of response mechanisms. *Nano Lett.* **2004**, *4*, 491–496. [CrossRef]
3. Matsuguchi, M.; Io, J.; Sugiyama, G.; Sakai, Y. Effect of NH$_3$ gas on the electrical conductivity of polyaniline blend films. *Synth. Met.* **2002**, *128*, 15–19. [CrossRef]
4. Bai, S.; Zhao, Y.; Sun, J.; Tian, Y.; Luo, R.; Li, D.; Chen, A. Ultrasensitive room temperature NH$_3$ sensor based on a graphene–polyaniline hybrid loaded on PET thin film. *Chem. Commun.* **2015**, *51*, 7524–7527. [CrossRef]
5. Wang, T.; Guo, Y.; Wan, P.; Zhang, H.; Chen, X.; Sun, X. Flexible transparent electronic gas sensors. *Small* **2016**, *12*, 3748–3756. [CrossRef]
6. Li, X.; Xu, J.; Jiang, Y.; He, Z.; Liu, B.; Xie, H.; Li, H.; Li, Z.; Wang, Y.; Tai, H. Toward agricultural ammonia volatilization monitoring: A flexible polyaniline/Ti$_3$C$_2$T$_x$ hybrid sensitive films based gas sensor. *Sens. Actuators B Chem.* **2020**, *316*, 128144. [CrossRef]
7. Kulkarni, S.; Navale, Y.; Navale, S.; Stadler, F.; Ramgir, N.; Patil, V. Hybrid polyaniline-WO$_3$ flexible sensor: A room temperature competence towards NH$_3$ gas. *Sens. Actuators B Chem.* **2019**, *288*, 279–288. [CrossRef]
8. Hien, H.T.; Giang, H.T.; van Hieu, N.; Trung, T.; van Tuan, C. Elaboration of Pd-nanoparticle decorated polyaniline films for room temperature NH$_3$ gas sensors. *Sens. Actuators B Chem.* **2017**, *249*, 348–356. [CrossRef]
9. Abdulla, S.; Mathew, T.L.; Pullithadathil, B. Highly sensitive, room temperature gas sensor based on polyaniline-multiwalled carbon nanotubes (PANI/MWCNTs) nanocomposite for trace-level ammonia detection. *Sens. Actuators B Chem.* **2015**, *221*, 1523–1534. [CrossRef]
10. Wu, Z.; Chen, X.; Zhu, S.; Zhou, Z.; Yao, Y.; Quan, W.; Liu, B. Enhanced sensitivity of ammonia sensor using graphene/polyaniline nanocomposite. *Sens. Actuators B Chem.* **2013**, *178*, 485–493. [CrossRef]

11. Wang, S.; Jiang, Y.; Liu, B.; Duan, Z.; Pan, H.; Yuan, Z.; Xie, G.; Wang, J.; Fang, Z.; Tai, H. Ultrathin Nb_2CT_x nanosheets-supported polyaniline nanocomposite: Enabling ultrasensitive NH_3 detection. *Sens. Actuators B Chem.* **2021**, *343*, 130069. [CrossRef]

12. Jha, R.K.; Wan, M.; Jacob, C.; Guha, P.K. Ammonia vapour sensing properties of in situ polymerized conducting PANI-nanofiber/WS_2 nanosheet composites. *New J. Chem.* **2018**, *42*, 735–745. [CrossRef]

13. Li, X.; Li, X.; Li, Z.; Wang, J.; Zhang, J. WS_2 nanoflakes based selective ammonia sensors at room temperature. *Sens. Actuators B Chem.* **2017**, *240*, 273–277. [CrossRef]

14. Perkins, F.K.; Friedman, A.L.; Cobas, E.; Campbell, P.; Jernigan, G.; Jonker, B.T. Chemical vapor sensing with monolayer MoS_2. *Nano Lett.* **2013**, *13*, 668–673. [CrossRef] [PubMed]

15. Late, D.J.; Doneux, T.; Bougouma, M. Single-layer $MoSe_2$ based NH_3 gas sensor. *Appl. Phys. Lett.* **2014**, *105*, 233103. [CrossRef]

16. Feng, Z.; Xie, Y.; Chen, J.; Yu, Y.; Zheng, S.; Zhang, R.; Li, Q.; Chen, X.; Sun, C.; Zhang, H.; et al. Highly sensitive $MoTe_2$ chemical sensor with fast recovery rate through gate biasing. *2D Mater.* **2017**, *4*, 025018. [CrossRef]

17. Liu, G.; Zhou, Y.; Zhu, X.; Wang, Y.; Ren, H.; Wang, Y.; Gao, C.; Guo, Y. Humidity enhanced ammonia sensing of porous polyaniline/tungsten disulfide nanocomposite film. *Sens. Actuators B Chem.* **2020**, *323*, 128699. [CrossRef]

18. Zhang, D.; Wu, Z.; Li, P.; Zong, X.; Dong, G.; Zhang, Y. Facile fabrication of polyaniline/multi-walled carbon nanotubes/molybdenum disulfide ternary nanocomposite and its high-performance ammonia-sensing at room temperature. *Sens. Actuators B Chem.* **2018**, *258*, 895–905. [CrossRef]

19. Qiu, L.; Wei, Y.; Pol, V.G.; Gedanken, A. Synthesis of α-$MoTe_2$ nanorods via annealing te-seeded amorphous $MoTe_2$ particles. *Inorg. Chem.* **2004**, *43*, 6061–6066. [CrossRef]

20. Panigrahi, P.; Hussain, T.; Karton, A.; Ahuja, R. Elemental substitution of two-dimensional transition metal dichalcogenides ($MoSe_2$ and $MoTe_2$): Implications for enhanced gas sensing. *ACS Sens.* **2019**, *4*, 2646–2653. [CrossRef]

21. Cho, S.; Kim, S.; Kim, J.H.; Zhao, J.; Seok, J.; Keum, D.H.; Baik, J.; Choe, D.H.; Chang, K.J. Phase patterning for ohmic homojunction contact in $MoTe_2$. *Science* **2015**, *349*, 625–628. [CrossRef] [PubMed]

22. He, H.Y.; He, Z.; Shen, Q. One-pot synthesis of non-precious metal RGO/1T'-$MoTe_2$: Cu heterohybrids for excellent catalytic hydrogen evolution. *Mater. Sci. Eng. B* **2020**, *260*, 114659. [CrossRef]

23. Chen, X.; Chen, X.; Ding, X.; Yu, X.; Yu, X. Gas-sensitive enhancement of rGO/HMWCNTs/PANI ternary composites. *IEEE Sens. J.* **2021**, *22*, 1905–1915. [CrossRef]

24. Trchová, M.; Šeděnková, I.; Tobolková, E.; Stejskal, J. FTIR spectroscopic and conductivity study of the thermal degradation of polyaniline films. *Polym. Degrad. Stab.* **2004**, *86*, 179–185. [CrossRef]

25. Yan, C.; Zou, L.; Short, R. Single-walled carbon nanotubes and polyaniline composites for capacitive deionization. *Desalination* **2012**, *290*, 125–129. [CrossRef]

26. Ginic-Markovic, M.; Matisons, J.G.; Cervini, R.; Simon, G.P.; Fredericks, P.M. Synthesis of new polyaniline/nanotube composites using ultrasonically initiated emulsion polymerization. *Chem. Mater.* **2006**, *18*, 6258–6265. [CrossRef]

27. Gavgani, J.N.; Hasani, A.; Nouri, M.; Mahyari, M.; Salehi, A.J.S. Highly sensitive and flexible ammonia sensor based on S and N co-doped graphene quantum dots/polyaniline hybrid at room temperature. *Sens. Actuators B Chem.* **2016**, *229*, 239–248. [CrossRef]

28. Fan, H.; Zhao, N.; Wang, H.; Xu, J.; Pan, F. 3D conductive network-based free-standing PANI–RGO–MWNTs hybrid film for high-performance flexible supercapacitor. *J. Mater. Chem. A* **2014**, *2*, 12340–12347. [CrossRef]

29. Saini, P.; Choudhary, V.; Singh, B.P.; Mathur, R.B.; Dhawan, S.K. Polyaniline–MWCNT nanocomposites for microwave absorption and EMI shielding. *Mater. Chem. Phys.* **2009**, *113*, 919–926. [CrossRef]

30. Andre, R.S.; Shimizu, F.M.; Miyazaki, C.M.; Riul, A., Jr.; Manzani, D.; Ribeiro, S.J.; Oliveira, O.N., Jr.; Mattoso, L.H.; Correa, D.S. Hybrid layer-by-layer (LbL) films of polyaniline, graphene oxide and zinc oxide to detect ammonia. *Sens. Actuators B Chem.* **2017**, *238*, 795–801. [CrossRef]

31. Bandgar, D.K.; Navale, S.T.; Navale, Y.H.; Ingole, S.M.; Stadler, F.J.; Ramgir, N.; Aswal, D.K.; Gupta, S.K.; Mane, R.S.; Patil, V.B. Flexible camphor sulfonic acid-doped $PAni$/α-Fe_2O_3 nanocomposite films and their room temperature ammonia sensing activity. *Mater. Chem. Phys.* **2017**, *189*, 191–197. [CrossRef]

32. Kulkarni, S.B.; Navale, Y.H.; Navale, S.T.; Ramgir, N.S.; Debnath, A.K.; Gadkari, S.C.; Gupta, S.K.; Aswal, D.K.; Patil, V.B. Enhanced ammonia sensing characteristics of tungsten oxide decorated polyaniline hybrid nanocomposites. *Org. Electron.* **2017**, *45*, 65–73. [CrossRef]

33. Tohidi, S.; Parhizkar, M.; Bidadi, H.; Mohamad-Rezaei, R.J.N. High-performance chemiresistor-type NH_3 gas sensor based on three-dimensional reduced graphene oxide/polyaniline hybrid. *Nanotechnology* **2020**, *31*, 415501. [CrossRef]

34. Wang, S.; Liu, B.; Duan, Z.; Zhao, Q.; Zhang, Y.; Xie, G.; Jiang, Y.; Li, S.; Tai, H. PANI nanofibers-supported Nb_2CTx nanosheets-enabled selective NH_3 detection driven by TENG at room temperature. *Sens. Actuators B Chem.* **2021**, *327*, 128923. [CrossRef]

35. Gong, J.; Li, Y.; Hu, Z.; Zhou, Z.; Deng, Y. Ultrasensitive NH_3 gas sensor from polyaniline nanograin enchased TiO_2 fibers. *J. Phys. Chem. C* **2010**, *114*, 9970–9974. [CrossRef]

36. Rigoni, F.; Drera, G.; Pagliara, S.; Perghem, E.; Pintossi, C.; Goldoni, A.; Sangaletti, L. Gas sensing at the nanoscale: Engineering SWCNT-ITO nano-heterojunctions for the selective detection of NH_3 and NO_2 target molecules. *Nanotechnology* **2016**, *28*, 035502. [CrossRef]

37. Qin, Y.; Wang, L.; Wang, X. A high performance sensor based on PANI/ZnTi-LDHs nanocomposite for trace NH_3 detection. *Org. Electron.* **2019**, *66*, 102–109. [CrossRef]

38. Xie, Y.; Wu, E.; Zhang, J.; Hu, X.; Zhang, D.; Liu, J. Gate-tunable photodetection/voltaic device based on BP/MoTe$_2$ heterostructure. *ACS Appl. Mater. Interfaces* **2019**, *11*, 14215–14221. [CrossRef]

39. Zhang, D.; Wu, Z.; Zong, X. Metal-organic frameworks-derived zinc oxide nanopolyhedra/S, N: Graphene quantum dots/polyaniline ternary nanohybrid for high-performance acetone sensing. *Sens. Actuators B Chem.* **2019**, *288*, 232–242. [CrossRef]